Structure of various KL^1 x-ray satellite lines of heavy atoms

Marek Polasik and Maja Lewandowska-Robak
Faculty of Chemistry, Nicholas Copernicus University, 87-100 Toruń, Poland
(Received 27 May 2004; published 4 November 2004)

Multiconfiguration Dirac-Fock calculations with the inclusion of the transverse (Breit) interaction and QED corrections have been carried out for Pd, Sn, Tb, Ta, Pb, and Th in order to obtain positions and intensities of various electric dipole, electric quadrupole, and magnetic dipole K x-ray diagram lines and of their KL^1 satellites. Theoretically constructed stick spectra have been presented together with synthesized spectra (the sum of the Lorentzian natural line shapes) for each studied element. Taking into account the existence of an L-shell hole in the $2s$ or $2p$ subshell, the effect of additional L-shell ionization on the shapes and structure of the K x-ray spectra has been examined. It has been observed that generally with increasing atomic number Z the shapes of particular satellite line groups tend to become smoother and to differ less from the shapes of appropriate diagram lines. Relations between the values of energy shifts of various satellite lines for each element and the changes of these relations with Z have also been studied. Additionally, the relations between the intensities of different diagram lines for each element have been systematically analyzed, likewise the changes with Z of the role of particular diagram lines. This study can be helpful in reliable and quantitative interpretation of many experimental K x-ray spectra of Pd, Sn, Tb, Ta, Pb, and Th induced in collisions with various projectiles.

DOI: 10.1103/PhysRevA.70.052502 PACS number(s): 32.30.Rj, 32.70.Jz, 32.70.Fw, 31.15.−p

I. INTRODUCTION

Numerous studies based on the interpretation of the K x-ray spectra have been performed in order to investigate the mechanism of the inner shell ionization in collision processes. Much research has been devoted to the determination of the L-shell ionization probability in near-central collisions from measured K x-ray spectra of multiply ionized target atoms with the atomic number $Z<30$ [1–22] and then, since 1987, also of target atoms with $Z>40$ [23–29]. In the 1990s Carlen and co-workers [30,31] developed this method so that it could be applied to the determination of the M-shell ionization probability in near-central collisions with light ions as projectiles. Yet, especially in the case of near-central collisions with energetic heavy ions, the multiple ionization of inner shells is highly probable and results in a very complex origin of the K x-ray spectra of target atoms. Thus to reliably interpret the experimental K x-ray spectra it is essential to include theoretical study on the effect of the multiple ionization of inner shells on the positions and shapes of respective x-ray lines. Such theoretical studies can be crucial in the interpretation of different collision processes in many fields, e.g., in atomic physics, solid-state physics, trace element analysis, laser physics, astrophysics, plasma and nuclear physics.

One of us (Polasik) has in recent years developed and used theoretical models enabling reliable descriptions of very complex x-ray spectra of target atoms induced in near-central collisions of the targets with energetic heavy ions. In his first study concerning the x-ray spectra of multiply ionized atoms [32] multiconfiguration Dirac-Fock (MCDF) calculations with the inclusion of the transverse (Breit) interaction, self-energy, and vacuum polarization corrections were performed for Pd in order to elucidate the structure of the $K\alpha_{1,2}L^nM^0$ satellite lines in its x-ray spectra (where in the symbols of the KL^nM^r type n and r indicate the number of the L- and M-shell holes, respectively, in the initial state). The measurement of the high-resolution x-ray spectra of Mo [23] inspired Polasik to carry out a theoretical simulation of these spectra using a model in which a spectrum was represented as a sum of the bands (which were the convolution of the sum of the Lorentzian natural line shapes with the Gaussian instrumental response) resulting from the transitions of the $K\alpha_{1,2}L^nM^0$ type [33]. The effect of the M-shell ionization was taken into account in a crude way by simply shifting a spectrum towards higher energies and applying larger Gaussian linewidths. In the next two papers of this series the MCDF method was successfully applied to an extensive and detailed study on the structure of the $K\alpha_{1,2}L^0M^r$ lines in Mo, Pd, and Ho [34], and also in a theoretical study on the structure of the $K\alpha_{1,2}L^1M^r$ lines in Pd [35].

The structure of the $K\beta$ lines in the x-ray spectra of mid-Z elements was systematically investigated by Polasik in [36], where the extensive MCDF studies on the structure of the $K\beta_{1,3}L^0M^r$ lines were performed for Mo, Pd, and La. The results of these calculations enabled a reliable description of the influence of additional holes in the M shell on the shapes and positions of the $K\beta_{1,3}L^0$ bands, which may be used in theoretical analysis of various experimental x-ray spectra generated in collisions with different ions. About ten years ago these results were applied together with previous ones to the theoretical analysis of the $K\alpha_{1,2}L^0M^r$ and the $K\beta_{1,3}L^0M^r$ x-ray spectra of Mo [37], Pd, and La [38] induced by O ions, where a different method of the analysis of very complex K x-ray spectra accompanying the ionization of the target atoms in near-central collisions with energetic heavy ions was used. In this method the measured $K\alpha$ and $K\beta$ spectra are simultaneously decomposed into the theoretical line profiles for the $K\alpha_{1,2}L^0M^r$ and the $K\beta_{1,3}L^0M^r$ transitions, constructed on the basis of the results of the MCDF calculations. The binomial distribution of holes in the M shell is assumed and the M-shell ionization probability per electron (p_M) is ex-

 ©2004 The American Physical Society

tracted from the best fit of the theoretical profiles to the analyzed spectrum. By then, it had been the only known way to extract p_M from complex K x-ray spectra induced by heavy ions.

Then, high-resolution spectra were measured for the $K\beta_2$ lines of Zr, Nb, Mo, Pd, and Pr induced by various kinds of projectiles [39–43]. Although the $K\beta_2M^1$ x-ray satellites were mostly resolved, reliable values of p_M were obtained due to the decomposition of the experimental spectra into the $K\beta_2$ diagram and satellite components which were constructed theoretically using the MCDF calculations. The theoretical profiles were fitted to the experimental spectra. From the relative yields of the $K\beta_2M^1$ satellites the appropriate experimental average M-shell ionization probabilities in near-central collisions were determined.

Recently [44], the results of extensive MCDF calculations of many K x-ray diagram lines and the corresponding KL^1M^0 satellite lines of Ta, Pb, and Th enabled reliable interpretation of measured K x-ray spectra, induced during near-central collisions with light and heavy projectiles. The considered collisions lead to nuclear reactions and owing to the MCDF calculations of the K x-ray line positions and intensities it was possible to decompose the measured spectra of a very complex origin into contributions from the target atom and the products of nuclear reactions, and then to get reliable information about the K x-ray cross sections and the L-shell ionization probabilities [44].

In this paper we have aimed to examine the effect of the L-shell ionization on the K x-ray spectra. We have also wanted to prove the reliability of the model applied to the calculations for various diagram and satellite lines and in such a wide range of the atomic number of the studied elements (from $Z=46$ for Pd to $Z=90$ for Th). Additionally, we have investigated how the role of respective diagram lines changes with Z. The study presented in this paper is a systematic study on the structure and shapes of satellite spectra, analyzing in detail the effect of removing a $2s$ and a $2p$ electron on the K x-ray spectra and attempting to explain all the observed relations for each studied element and their changes with Z. We believe that our work can be very helpful in reliable and quantitative interpretation of various K x-ray spectra induced by light or heavy projectiles. Our results can also be useful in the analysis of the observed K x-ray spectra of other multiply ionized heavy atoms and can contribute to better understanding of collision processes.

II. MCDF CALCULATIONS

The MCDF method, used in the present study, has been described in detail in many papers [45–52]. Therefore only a brief description will be given here, pointing out the essential details. Within the MCDF scheme the effective Hamiltonian for an N-electron system is expressed by

$$H = \sum_{i=1}^{N} h_D(i) + \sum_{j>i=1}^{N} C_{ij}, \tag{1}$$

where $h_D(i)$ is the Dirac operator for ith electron and the terms C_{ij} account for electron-electron interactions and come from the one-photon exchange process. The latter are a sum of the Coulomb interaction operator (due to longitudinally polarized photons) and the transverse Breit operator (due to transversely polarized photons).

In the MCDF method an atomic state function (ASF) with the total angular momentum J and parity p is assumed in the multiconfigurational form:

$$\Psi_s(J^p) = \sum_m c_m(s)\Phi(\gamma_m J^p), \tag{2}$$

where $\Phi(\gamma_m J^p)$ are configuration state functions (CSF's), $c_m(s)$ are the configuration mixing coefficients for state s, and γ_m represents all information required to uniquely define a certain CSF.

Various versions of MCDF calculations are distinguished by the choice of the form of the energy functional. In the calculations in the standard optimal-level version of MCDF (MCDF-OL) for a particular state we get the optimal energy, the optimal set of one-electron spinors, and the optimal set of the CSF mixing coefficients $\{c_m(s)\}$. The application of the MCDF-OL version to the calculations of the transition probabilities should take into account the fact of nonorthogonality of the spinors corresponding to the pairs of initial and final states. Since the use of the MCDF-OL method demands a separate MCDF-OL calculation for each state and in the theoretical studies on x-ray spectra in many cases we must consider transitions occurring between hundreds of states, the MCDF-OL calculations are very time consuming. Thus to avoid such difficulties some other methods (different from MCDF-OL) are applied to the study on the transition probabilities and energies. The main feature of those methods is the fact that a common set of the orbitals for all the initial and final states is used. There are two standard schemes based on this idea, namely the average-level version of MCDF (MCDF-AL) and the extended average-level version of MCDF (MCDF-EAL). Yet, preliminary test calculations have shown that MCDF-AL and MCDF-EAL schemes are not accurate enough in some cases. The reason for this seems to lie in the fact that the energy functional does not take into account the different number of the initial and final states. Therefore the orbitals obtained in these schemes in a sense favor those states (initial or final) which are more numerous. In order to make the MCDF calculations of the transition energies and probabilities as reliable as possible, in the present study we use the modified special average-level version of MCDF calculations (MCDF-MSAL), proposed in Refs. [36,37]. In this version the energy functional to some extent enables the compensation of the above-mentioned imbalance and is expressed by

$$E = E_{opt} + \sum_a \overline{q_a}\epsilon_a S(a,a) + \sum_{\substack{a,b \\ a\neq b}} \epsilon_{a,b} S(a,b), \tag{3}$$

where $\overline{q_a}$ is the generalized occupation number for the orbital a, ϵ_a and ϵ_{ab} are the Lagrange multipliers, $S(a,b)$ is the overlap integral, and E_{opt} [36,37] is taken in the form

$$E_{opt} = \frac{1}{\lambda + 1}\left(\frac{\lambda}{n_i}\sum_{i=1}^{n_i} H_{ii} + \frac{1}{n_f}\sum_{f=1}^{n_f} H_{ff}\right), \tag{4}$$

where H_{ii} and H_{ff} are the diagonal contributions to the Hamiltonian matrix, the first sum runs over all the initial CSF's (n_i), and the second sum runs over all the final CSF's (n_f). The presence of a factor λ in formula (4) in the simplest way enables the compensation of the difference in the quality of description of initial and final states, which is the main problem in reliable theoretical (MCDF) study on the structure of the KL^nM^r lines in the x-ray spectra.

It is easy to notice that if λ were equal to 1 we would obtain a formula in which the compensation of exaggerating the contribution of the more numerous states (initial or final) to the energy functional is complete. As a result, we would get a good reproduction of the relative positions of the spectral lines. However, for $\lambda=1$ the calculated (diagram and satellite) transition energies would be shifted for the considered kinds of lines (like, e.g., $K\alpha_{1,2}L^nM^r$, $K\beta_{1,3}L^nM^r$, or $K\beta_2L^nM^r$) by similar amounts with respect to the experimental transitions. Thus there must be some optimum values of λ for particular line kinds. Test calculations have shown that these optimum values [36], depending strongly on the kind of spectral line, are rather weakly dependent on the atom. It is worth emphasizing that this simple formula, with specific values of λ, has proved to reproduce very well experimental diagram (see Refs. [31,37,38]) and satellite (see Ref. [31]) lines for medium Z atoms. Therefore formula (4) provides a simple and effective way of calculating the absolute positions of spectral lines.

The functional used in this paper has been successfully applied in the extensive MCDF study on the structure of the $K\alpha_{1,2}L^nM^r$ and $K\beta_{1,3}L^nM^r$ lines in the x-ray spectra of Mo [37], Pd, and La [38] induced in near-central collisions with O ions, as well as $K\beta_{1,3}L^nM^r$ and $K\beta_2L^nM^r$ lines of Mo induced by C ions [42]. It has also been used in the study on the $K\beta_2L^nM^r$ lines of Zr, Mo, and Pd induced by proton and photon beams [39], the $K\beta_2L^nM^r$ lines of Zr, Nb, Mo, and Pd generated by electrons [40] and by C ions [43], and also the $K\alpha_{1,2}L^nM^r$, $K\beta_{1,3}L^nM^r$ [53], and $K\beta_2L^nM^r$ [41] lines of Zr, Mo, Pd, and Pr generated by He ions. Recently, the MCDF-MSAL method has been applied to the calculations of many different K x-ray diagram lines and their KL^1M^0 satellite lines for Ta, Pb, and Th. The results of those calculations were crucial in the analysis of the K x-ray spectra of the above atoms induced by He, C, O, and Ne projectiles [44].

Apart from the transverse (Breit) interaction we have included in our study two types of QED energy corrections (self-energy and vacuum polarization), which are significant in the case of heavy atoms [46,47,50–52]. The formulas for the transition matrix elements and spontaneous emission probabilities can be found in the work of Grant [45]. The calculations have been performed for both Coulomb and Babushkin [45,54] gauges. In the nonrelativistic limit the Coulomb gauge formula for the electric dipole transitions yields the dipole velocity expression while the Babushkin formula gives the dipole length expression [45].

III. RESULTS AND DISCUSSION

The K x-ray lines studied here can all be denoted with the use of the symbols of the KL^n type, where n indicates the number of electrons removed in the initial state from the L shell. Since the x rays produced in a radiative decay of singly ionized atoms are represented in the spectra by the diagram lines, the K diagram lines appear when the atom has in the initial state only one hole in the K shell (i.e., $1s$) and no electrons from higher shells removed. Such states are denoted $1s^{-1}$. The K diagram lines can be referred to as of the KL^0 type.

In Fig. 1 we have shown 13 K x-ray diagram lines for heavy atoms, appearing in the least complicated case, when a $1s$ electron is removed from a neutral atom the ground state of which has a closed-shell relativistic configuration, i.e., only empty or completely filled relativistic subshells. On the basis of selection rules it can easily be noticed that in Fig. 1 there are eight electric dipole, $E1$, x-ray transitions, for which the change of the quantum numbers of the orbital angular momentum of the electron filling the K-shell hole, l, and of the total angular momentum of the state, J, must be: $\Delta l=-1,1$ and $\Delta J=-1,0,1$ (where transitions $J=0\rightarrow J=0$ are forbidden). Transitions of the $E1$ type are called allowed transitions and they have the highest intensities. The $E1$ transitions studied here are: $K\alpha_2$ and $K\alpha_1$ (both from the initial states of the ion with one hole in the $1s$ subshell to the final state where an electron from the $2p$ subshell has filled that hole, denoted thus $1s^{-1}\rightarrow 2p^{-1}$), $K\beta_3$ and $K\beta_1$ (where the initial K-shell hole is filled by an electron from the $3p$ subshell, denoted $1s^{-1}\rightarrow 3p^{-1}$), $K\beta_2^{II}$ and $K\beta_2^{I}$ ($1s^{-1}\rightarrow 4p^{-1}$), and KO_2 and KO_3 ($1s^{-1}\rightarrow 5p^{-1}$). In Fig. 1 there are also less intensive transitions, called forbidden, of the electric quadrupole, $E2$, and magnetic dipole, $M1$, types. For $E2$ transitions there must be: $\Delta l=-2,0,2$ and $\Delta J=-2,-1,0,1,2$ (where transitions $J=0\rightarrow J=0$, $J=1/2\rightarrow J=1/2$, $J=0\rightarrow J=1$, and $J=1\rightarrow J=0$ are not allowed) and for $M1$ transitions there must be: $\Delta l=0$, and $\Delta J=-1,0,1$ (where transitions $J=0\rightarrow J=0$ are not allowed). There are also four diagram $E2$ lines, i.e., $K\beta_5^{II}$ and $K\beta_5^{I}$ ($1s^{-1}\rightarrow 3d^{-1}$), and $K\beta_4^{II}$ and $K\beta_4^{I}$ ($1s^{-1}\rightarrow 4d^{-1}$). The remaining line from Fig. 1, denoted $K\alpha_3$ ($1s^{-1}\rightarrow 2s^{-1}$), is of the $M1$ type.

We have performed for Pd, Sn, Tb, Ta, Pb, and Th the MCDF-MSAL (see Sec. II) calculations of the energies and probabilities of the 13 K x-ray diagram transitions (excluding $KO_{2,3}$ lines for Pd, which does not have the $5p$ subshell occupied) and of their KL^1 satellite transitions, i.e., the ones from the initial states with a K-shell and an L-shell electrons (and no electrons from higher shells) removed. The results of the MCDF calculations of energies, E, and relative (with respect to the strongest, $K\alpha_1$, line) intensities of the K x-ray diagram lines of Pd, Tb, Pb, and Th are presented in Table I. The lines are arranged according to the order of increasing energy. The relative intensities have been calculated using Coulomb [45] and Babushkin [54] gauges. It is worth noting that although the intensity values depend on the gauge used (which reflects the approximated character of the applied theoretical model), the structure of the groups of lines and of the whole theoretical spectrum usually does not depend significantly on the choice of the gauge. As can be found from Table I the calculated relative diagram line intensities reproduce reliably the experimental values [55]. The energy values are also in an excellent agreement with the experimental

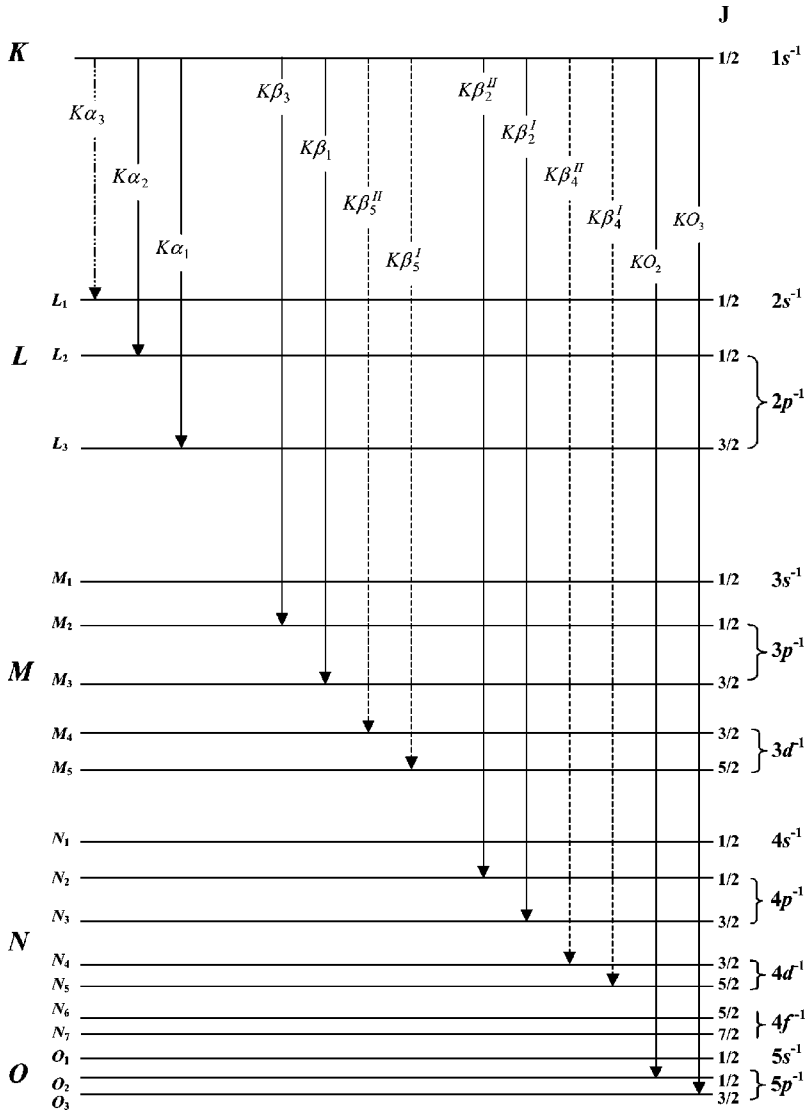

FIG. 1. Outline of the studied K x-ray diagram transitions (in Siegbahn notation) for heavy atoms in the case of the closed-shell (before removing a K-shell electron) ground state of the atom. On the left side of the figure associated initial K and various final vacancies in the x-ray energy levels are given. On the right side the notation emphasizes the existence of holes in a quantum-mechanical approach. For each level the values of the total angular momentum of the state J have been also presented. The transitions of electric dipole type are represented as solid lines, of electric quadrupole type as dashed lines, and of magnetic dipole type as dotted and dashed lines.

data of Bearden [56] (discrepancies usually of the order of 1 eV) and in a good agreement with the theoretical and experimental data presented in Deslattes *et al.* [57].

A detailed discussion of the results obtained for the diagram lines is presented in the Appendix. From that discussion it can be concluded that in calculations for the x-ray lines of heavy elements much more transitions have to be taken into account than in the case of light elements, because for the latter high shells are either unoccupied or the $E1$ and $E2$ transitions occurring from them have very small intensities and generally all the transitions of types other than $E1$ are very weak, as well.

A. KL^1 satellite line structure

In Figs. 2–7 both stick and synthesized spectra for Pd, Sn, Tb, Ta, Pb, and Th are shown. In the stick spectra, on the basis of the MCDF calculations results (with the use of Coulomb [45] gauge), we have presented the energies of respective transitions (the positions of the sticks) with the relative intensities of the transitions multiplied by the degeneracies, i.e., $2J+1$, of the initial states (the heights of the sticks). The synthesized spectra (dashed lines) for all the cases have been constructed as the sum of the Lorentzian natural line shapes with the appropriate natural linewidths taken from Ref. [58]. In every figure there are three boxes. Each of them presents the spectra for particular lines. The bottom box is always for the $K\alpha_2$ and $K\alpha_1$ lines, the middle one for the $K\beta_3$ and $K\beta_1$ lines, and the top one for the $K\beta_5$, $K\beta_2$, $K\beta_4$, and (if applicable) $KO_{2,3}$ lines. Unfortunately, because of their very small intensity the extremely weak forbidden $K\alpha_3$ lines cannot be seen in the spectra of any of the investigated atoms. Also the $KO_{2,3}$ lines in the case of Sn are too weak to be visible in the spectra. As for the very weak $K\beta_4$ lines, their contributions have been included in the spectra of all the atoms and they affect the shapes of the theoretical spectra. Yet, only for the K x-ray diagram line spectra of the two heaviest of the studied elements, Pb and Th, they are significant enough to be identifiable as a slight deformation of the right shoulder of the $K\beta_2$ diagram bands (really small $K\beta_4$ sticks can be noticed in these spectra, too).

Every box includes four spectra. In the first, bottom, spectrum there are diagram lines and in the remaining spectra—their KL^1 satellite lines. The second spectrum is for the KL^1

TABLE I. Results of the MCDF calculations of the K x-ray diagram line energies (in eV), E, and relative (with respect to the $K\alpha_1$ line) intensities, I_{calc} (where upper values correspond to Coulomb gauge [45] and the bottom ones to Babushkin gauge [54]) for Pd, Tb, Pb, and Th. For comparison, experimental relative (with respect to the $K\alpha_1$ line) intensity values (in eV), I_{exp}, taken from Ref. [55] have been given. For the lines of the $K\beta_5$, $K\beta_2$, $K\beta_4$, and $KO_{2,3}$ kinds I_{exp} values concern added values for both lines in each of the pairs of lines. Thus to compare I_{exp} with I_{calc} one has to add the appropriate two values of I_{calc}, both in Coulomb or Babushkin gauge (e.g., in the case of the $K\beta_5$ lines I_{calc} for the $K\beta_5^I$ line and I_{calc} for the $K\beta_5^{II}$ line).

	$_{46}$Pd			$_{65}$Tb			$_{82}$Pb			$_{90}$Th		
Transition	E	I_{calc}	I_{exp}	E	I_{calc}	I_{exp}	E	I_{calc}	I_{exp}	E	I_{calc}	I_{exp}
$K\alpha_3$	20746.9	0.000019 0.000019		43287.9	0.00019 0.00019	0.00019 ±0.00001	72135.7	0.00106 0.00097	0.000926 ±0.000034	89175.6	0.00224 0.00196	0.0019 ±0.0001
$K\alpha_2$	21020.3	0.53062 0.52949	0.530 ±0.022	43744.0	0.57482 0.55820	0.562 ±0.018	72805.2	0.67281 0.59678	0.600 ±0.018	89958.0	0.74953 0.62104	0.619 ±0.019
$K\alpha_1$	21177.1	1.00000 1.00000	1.00	44481.0	1.00000 1.00000	1.00	74967.9	1.00000 1.00000	1.00	93348.2	1.00000 1.00000	1.00
$K\beta_3$	23791.4	0.09021 0.08989	0.0845 ±0.0035	50227.6	0.10912 0.10430	0.103 ±0.004	84449.6	0.13515 0.11304	0.121 ±0.004	104820.4	0.15201 0.11613	0.124 ±0.004
$K\beta_1$	23819.2	0.17558 0.17447	0.163 ±0.007	50384.2	0.20647 0.20181	0.199 ±0.006	84936.5	0.22402 0.21818	0.232 ±0.007	105603.3	0.22973 0.22516	0.236 ±0.007
$K\beta_5^{II}$	24010.6	0.00056 0.00053		50717.2	0.00166 0.00162		85422.5	0.00330 0.00305		106161.6	0.00438 0.00384	
$K\beta_5^{I}$	24015.8	0.00079 0.00074	0.00110 ±0.00006	50754.4	0.00219 0.00214	0.00328 ±0.00015	85523.9	0.00398 0.00367	0.00675 ±0.00030	106319.3	0.00503 0.00441	0.00837 ±0.00037
$K\beta_2^{II}$	24297.0	0.01502 0.01480		51673.1	0.02479 0.02352		87238.2	0.03293 0.02737		108474.7	0.03875 0.02926	
$K\beta_2^{I}$	24301.1	0.02889 0.02840	0.0397 ±0.0016	51713.0	0.04720 0.04568	0.0663 ±0.0021	87357.5	0.05642 0.05402	0.0846 ±0.0024	108677.4	0.06142 0.05892	0.0903 ±0.0026
$K\beta_4^{II}$	24347.9	0.000064 0.000070		51838.2	0.00040 0.00041		87569.6	0.00090 0.00084		108933.8	0.00130 0.00114	
$K\beta_4^{I}$	24348.2	0.000088 0.000096	0.00013 ±0.00007	51855.9	0.00052 0.00052	0.00084 ±0.00043	87591.7	0.00108 0.00101	0.0019 ±0.0009	108971.0	0.00149 0.00131	0.0024 ±0.0012
KO_2				51973.1	0.00393 0.00372		87905.6	0.00643 0.00534		109422.1	0.00914 0.00675	
KO_3				51979.3	0.00745 0.00717	0.0088 ±0.0009	87927.2	0.01068 0.01020	0.015 ±0.002	109467.7	0.01369 0.01349	0.020 ±0.003

satellite lines where the additional hole is in the $2s$ subshell (i.e., accompanying $1s^{-1}2s^{-1} \rightarrow X^{-1}2s^{-1}$ transitions, where X represents different subshells, depending on the line). In the third spectrum there are the KL^1 satellite lines where the additional hole is in the $2p$ subshell ($1s^{-1}2p^{-1} \rightarrow X^{-1}2p^{-1}$). The fourth spectrum in each box is the summary spectrum and presents all appropriate satellite lines of the KL^1 type, i.e., $1s^{-1}L^{-1} \rightarrow X^{-1}L^{-1}$ transitions, where L represents the $2s$ or $2p$ subshells. In this last spectrum the transitions from the states with a hole in the $2s$ or $2p$ subshells have been statis-

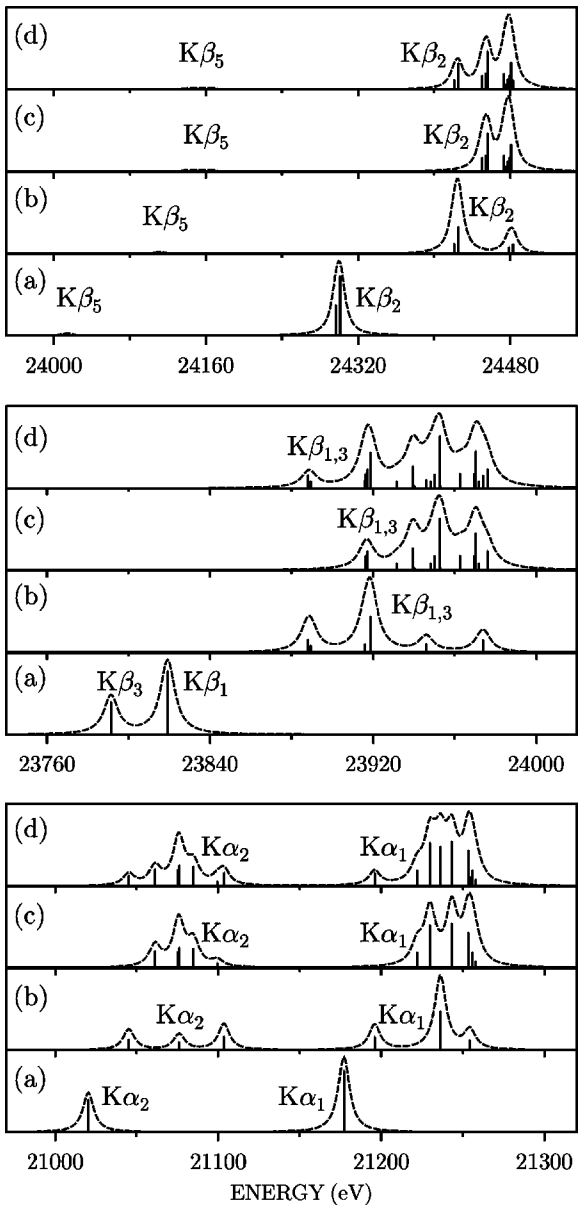

FIG. 2. Calculated stick (line positions with their relative intensities) and synthesized spectra (the sum of the Lorentzian components, dashed lines) of Pd for the K x-ray diagram transitions and the KL^1 satellite transitions. In all three boxes (a) is the diagram line spectrum, (b) is the satellite spectrum for the initial states with an additional 2s hole, (c) is the satellite spectrum for the initial states with an additional 2p hole and (d) is the summary satellite spectrum [(b) and (c)]. The diagram lines (and the corresponding KL^1 satellite lines) in the bottom box are the $K\alpha_{1,2}$ lines ($1s^{-1}\rightarrow 2p^{-1}$), in the middle box the $K\beta_{1,3}$ lines ($1s^{-1}\rightarrow 3p^{-1}$) and in the top box the $K\beta_5$ ($1s^{-1}\rightarrow 3d^{-1}$) and $K\beta_2$ ($1s^{-1}\rightarrow 4p^{-1}$) lines.

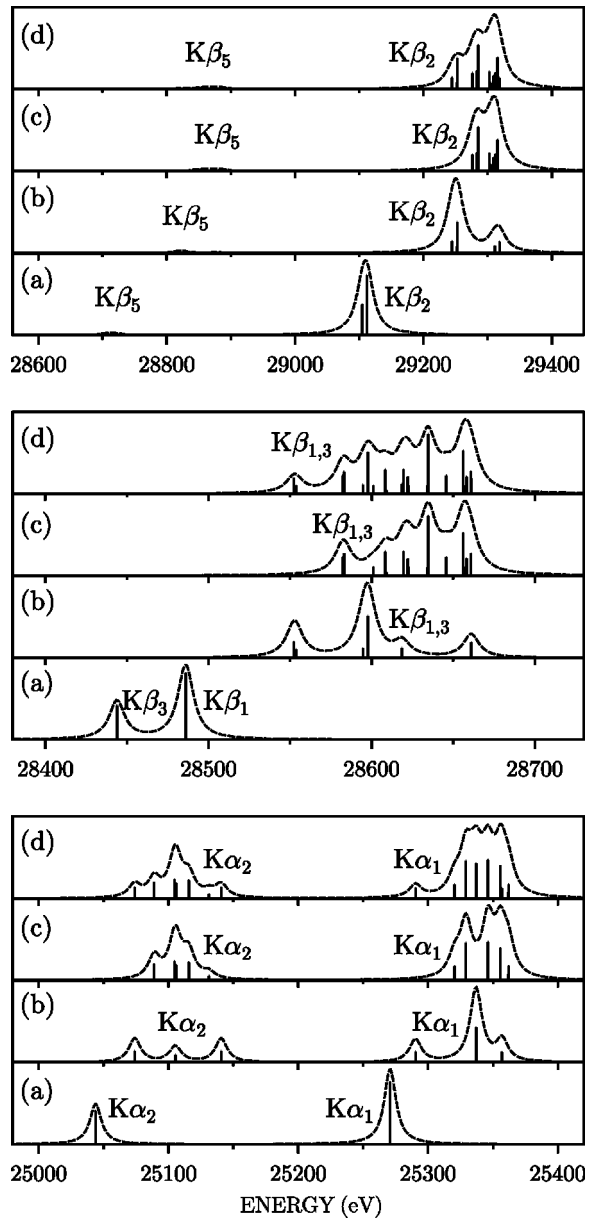

FIG. 3. As in Fig. 2, but for the spectra of Sn.

tically added. The summary spectra have been constructed under the assumption that the populations of the 2s- and 2p-hole states depend only on how many ways of creating a particular (2s or 2p) hole in the initial state there are. Thus there is a bigger contribution to the summary spectra from the 2p-hole states than from the 2s-hole states. We have not considered the influence of Coster-Kronig transitions, due to which the contribution of the 2p-hole states is even bigger than it has been assumed here.

It is worth noting that removing an additional electron induces a dramatic increase in the overall number of transitions and that in the satellite spectra in Figs. 2–7 there are groups of particular lines distributed widely around an average position. Because of that the shapes of satellite line spectra are different from the shapes of the corresponding diagram line spectra. The estimate of the effect of additional L-shell ionization on the structure and shapes of the K x-ray spectra can be made on the basis of the analysis of Figs. 2–7.

It should also be stressed that in our simulation of the theoretical x-ray spectra as the sum of the Lorentzian natural line shapes the appropriate natural linewidths (ranging in our case from about 8 to about 99 eV [58] and thus having a significant effect on the shapes) are used for each element

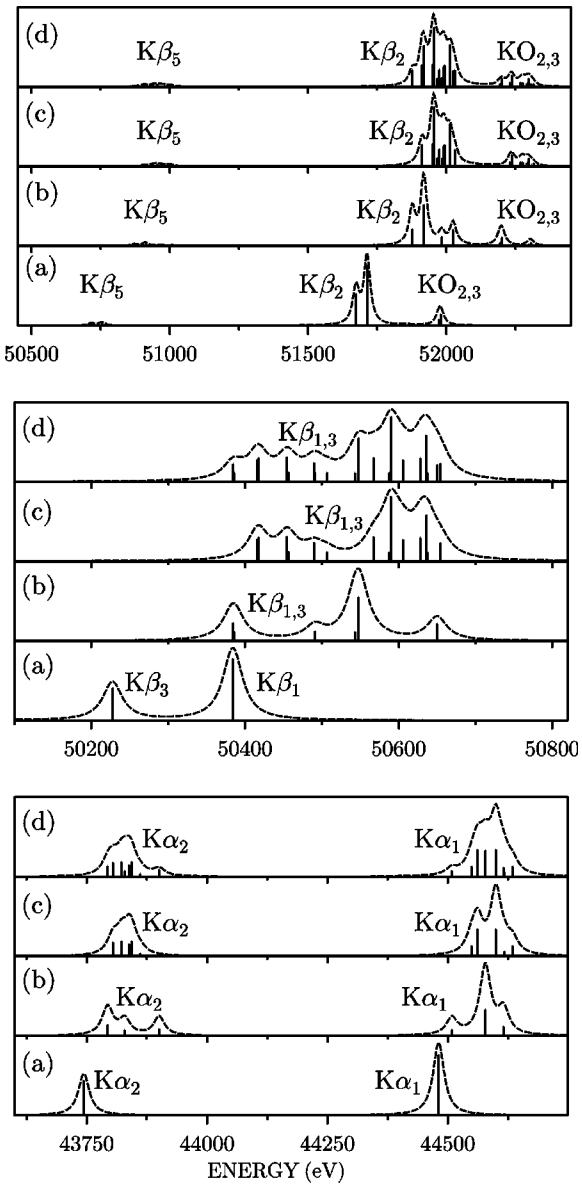

FIG. 4. As in Fig. 2, but for the spectra of Tb. In the top box additionally the $KO_{2,3}$ ($1s^{-1} \rightarrow 5p^{-1}$) diagram lines (and the corresponding KL^1 satellite lines) are presented.

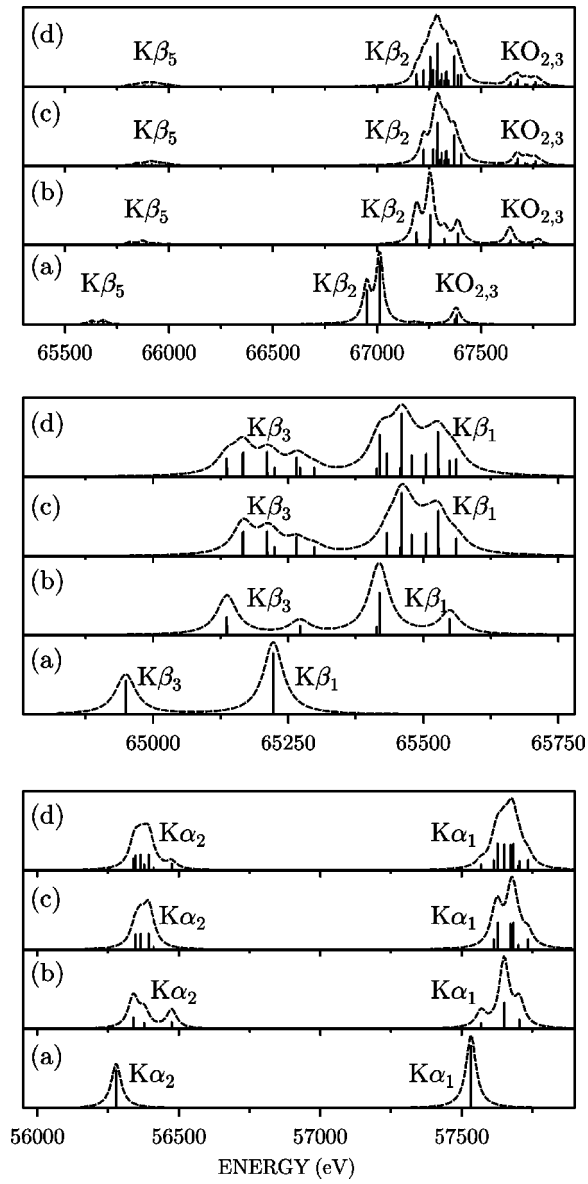

FIG. 5. As in Fig. 4, but for the spectra of Ta.

and each line. Our purpose has been to provide a universal characteristic of the natural shape of the spectra, which could be experimentally obtained with an ideal instrument. It has been shown [33,37,38] that the theoretical spectra after the convolution of the sum of the Lorentzian natural line shapes with the Gaussian instrumental response (the latter depending on the equipment used) are in an excellent agreement with the spectra measured with any kind of high-resolution instrument. Our theoretical spectra are also close to the experimental ones and including the instrumental response in our simulation would generally only smooth the shapes of the spectra. Thus our spectra enable foreseeing many details of the measured spectra, such as the separability of particular bands.

1. Pd (*Z*=46)

From Fig. 2 it can be seen that in the case of Pd (the lightest of the studied elements) the $K\alpha_2$ and $K\alpha_1$ diagram lines are well resolved, while the $K\beta_3$ and $K\beta_1$ diagram lines are resolved worse and the $K\beta_2^{II}$ and $K\beta_2^{I}$ diagram lines are not resolved. On the basis of Fig. 2 we cannot say much about the weak $K\beta_5$ lines.

The shapes of the KL^1 satellite lines of Pd are significantly different from the shapes of the corresponding diagram lines. It can be seen that generally in each satellite spectrum in Fig. 2 the sticks are widely distributed and they have also various intensities. Only in the case of the $K\beta_2$ lines the sticks are separated into groups. Both stick and synthesized spectra of the satellite lines for the $1s^{-1}2s^{-1}$ initial states are quite different from the spectra of the satellite lines for the $1s^{-1}2p^{-1}$ initial states. The stick spectra for the initial states with a $2s$ hole are for instance more scattered

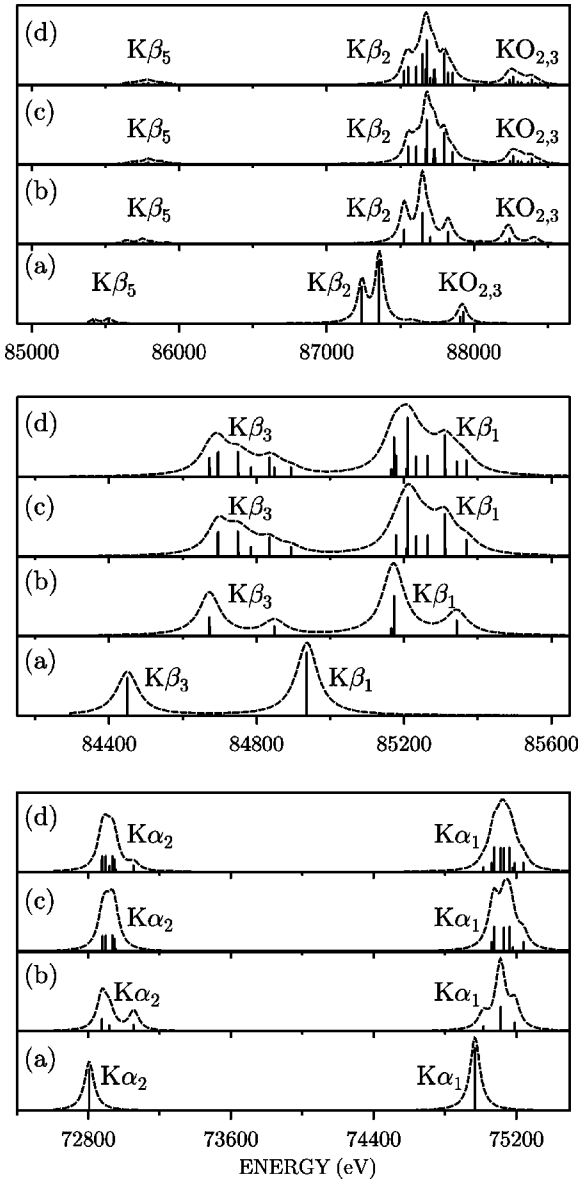

FIG. 6. As in Fig. 4, but for the spectra of Pb. In the top box, on the right shoulder of the $K\beta_2$ diagram band a small contribution from the $K\beta_4$ lines can be seen.

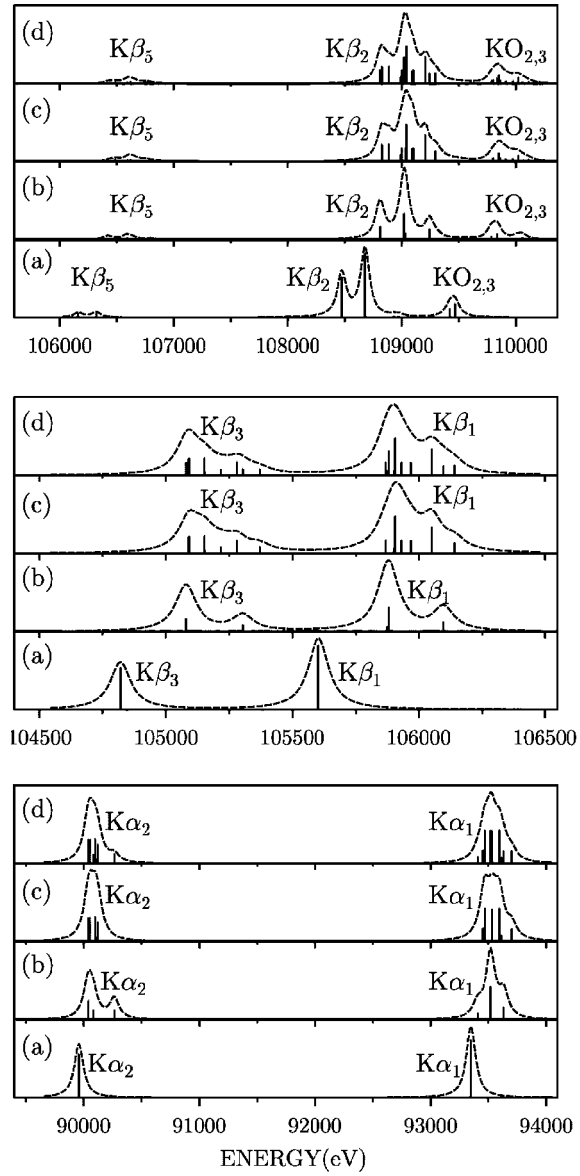

FIG. 7. As in Fig. 6, but for the spectra of Th. The contribution from the $K\beta_4$ lines on the right shoulder of the $K\beta_2$ diagram band is more visible than for Pb.

than those for the initial states with a $2p$ hole. In all the spectra there are also much fewer satellite lines of significant intensities in the case of the initial states with a $2s$ hole than for the initial states with a $2p$ hole. The summary spectra are similar to the spectra for the $1s^{-1}2p^{-1}$ initial states, due to the bigger contribution from the states with a $2p$ hole than from the states with a $2s$ hole.

The groups of the $K\alpha_2L^1$ and $K\alpha_1L^1$ satellite lines are well resolved, but similar pairs of groups of satellite lines (i.e., accompanying the transitions in which the K-shell holes are filled by electrons from the same nonrelativistic subshell, e.g., $3p$ for the pair of the $K\beta_3L^1$ and $K\beta_1L^1$ line groups) are not resolved into appropriate two groups.

2. Th ($Z=90$)

In the case of the heaviest of the analyzed elements—Th (Fig. 7)—in comparison with Pd there is first a difference in the number of diagram and satellite lines, as in the top box for Th we can observe $KO_{2,3}$ lines (accompanying the transitions from the $5p$ subshell, which is unoccupied in Pd). Besides, the $K\beta_5$ lines are more pronounced than in Pd and even the intensities of the $K\beta_4$ lines are strong enough to be visible in the spectra. Moreover, the $K\alpha_2$ and $K\alpha_1$ diagram lines, as well as the $K\beta_3$ and $K\beta_1$ diagram lines are well resolved, whereas the $K\beta_5^{II}$ and $K\beta_5^{I}$ diagram lines and also $K\beta_2^{II}$ and $K\beta_2^{I}$ diagram lines are resolved worse. The KO_2 and KO_3 diagram lines are not resolved.

As for the synthesized satellite spectra, all the bands in Th are wider than their counterparts in Pd (because of larger absolute distances between the first and the last line in a band). At the same time, in Th not only the $K\alpha_2L^1$ and $K\alpha_1L^1$ bands, but also the $K\beta_3L^1$ and $K\beta_1L^1$ bands are well resolved. The remaining satellite lines are not resolved into

appropriate two bands in most cases. All the synthesized spectra of Th satellite lines for the initial states with a $2p$ hole are very similar to the summary spectra, but the satellite line spectra for the $1s^{-1}2s^{-1}$ initial states are not very different from them, either (although the bands are more structured than for the $1s^{-1}2p^{-1}$ initial states). Contrary to Pd, the shapes of Th $K\alpha_{1,2}L^1$ satellite lines for the $1s^{-1}2p^{-1}$ initial states and in the summary spectrum are quite similar to the shapes of the $K\alpha_{1,2}$ diagram lines (but the satellite bands are of course much wider). This is a result of much larger natural linewidths of Th in comparison with Pd. Also the synthesized spectrum of the $K\alpha_{1,2}L^1$ lines for the $1s^{-1}2s^{-1}$ initial states and all the synthesized spectra of the $K\beta_{1,3}L^1$ lines differ less than in the case of Pd from the diagram line spectra. Generally, the shapes of all Th satellite spectra differ much (in terms of shapes and structure) from those for Pd, especially in the case of the $K\beta_{1,3}L^1$ and $K\beta_2L^1$ spectra. As for Th $K\alpha_{1,2}L^1$ bands, it can be said that their shapes are smoother than in Pd (because of larger natural linewidths).

Focusing on Th satellite stick spectra only, we can see that generally the distribution of the sticks in Th is different from that in Pd. In comparison with Pd the sticks are more widely distributed (larger distances between the first and the last line in a band) for all the kinds of Th satellite lines, which is directly connected with the increase of the role of relativistic effects. Yet, the increase of Z causes the energy range of Th spectra to be about six times bigger than for Pd. Therefore, for example in the case of Th $K\alpha_{1,2}L^1$ lines, the sticks form clearly separated two groups, inside which they seem to be closer to each other than in Pd (although in fact the distances are bigger). A very significant change of the structure for Th with respect to Pd can be also observed in the case of the $K\beta_2L^1$ lines, for which the sticks are much more scattered in Th than in Pd.

3. Sn ($Z=50$), *Tb* ($Z=65$), *Ta* ($Z=73$), *and Pb* ($Z=82$)

Analyzing now all Figs. 2–7 we can notice that there is a gradual change of the structure and shapes of the spectra from Pd through Sn, Tb, Ta, and Pb to Th.

The spectra for Sn (Fig. 3) are very similar to those for Pd. The most pronounced, but still small, differences between the spectra of these two elements are in the satellite spectra in the cases of the $K\beta_{1,3}L^1$ and $K\beta_2L^1$ lines, both for the initial states with a $2p$ hole and the summary spectra, where in Sn the synthesized spectra are smoother (larger natural linewidths) than for Pd.

The spectra for the next studied element—Tb (Fig. 4)—are more similar to Pd than to Th only in the cases of the $K\beta_{1,3}L^1$ lines in the spectrum for the initial $1s^{-1}2p^{-1}$ states and in the summary spectrum, but even in these spectra the sticks are significantly more scattered than in Pd and Sn. Also the shape of the $K\beta_{1,3}L^1$ line spectrum for the initial states with a $2s$ hole is remarkably different from the spectrum for Pd and Sn. Other satellite line spectra seem to resemble rather Th spectra, especially in the case of the $K\alpha_2L^1$ line spectra, the bands of which are significantly smoother than in Pd or Sn. The sticks in all Tb spectra are generally more scattered than in Sn and Pd.

The remaining elements under study—Ta and Pb—have spectra clearly resembling Th more than Pd. For Ta (Fig. 5) the shapes of the spectra do not change significantly in comparison with Tb in the cases of the spectra for the $K\beta_2L^1$ lines (apart from the summary spectrum, the shape of which is remarkably smoother than for Tb), $K\alpha_{1,2}L^1$, and $KO_{2,3}L^1$ lines. The distribution of the sticks is similar to that in Tb in all the spectra of the $K\alpha_2L^1$ and $KO_{2,3}L^1$ lines and also in the case of the $K\alpha_1L^1$ and $K\beta_2L^1$ spectra for the initial states with an additional $2s$ or $2p$ hole. The most pronounced change in comparison with Tb is observed for the $K\beta_{1,3}L^1$ summary spectrum and the $K\beta_{1,3}L^1$ spectrum for the $1s^{-1}2p^{-1}$ initial states. In these spectra the lines are resolved in Ta into two groups corresponding to the $K\beta_3L^1$ and to the $K\beta_1L^1$ lines, so that there is a separate shape for each of these line groups and also the sticks form clearly two, though widely distributed, groups. Yet, the $K\beta_{1,3}L^1$ spectrum for the $1s^{-1}2s^{-1}$ initial states is more similar to Tb (both in terms of shapes and sticks) and the separation into the two groups is not so clear.

All the spectra of Pb (Fig. 6) are very similar to those of Th. As for the synthesized spectra, the shape of Pb $K\alpha_1L^1$ spectrum for the $1s^{-1}2p^{-1}$ initial states is a little less smooth than in Th. Conversely, in the $K\beta_2L^1$ spectrum for the $1s^{-1}2p^{-1}$ initial states and in the $K\beta_2L^1$ summary spectrum the shapes for Pb are smoother than for Th. The distribution of the sticks generally does not differ much from that in Th, especially in the cases of the spectra for the $1s^{-1}2s^{-1}$ initial states.

In comparison with Ta, the shapes of Pb $K\alpha_2L^1$ spectrum for the initial states with a $2s$ hole and also the $K\alpha_1L^1$ and the $K\beta_{1,3}L^1$ spectra—both summary and for an additional $2p$ hole—are slightly smoother in Pb. The shapes of all the $K\beta_2L^1$ spectra differ a little from those for Ta, so that the summary $K\beta_2L^1$ spectrum is less smooth for Pb than for Ta. In the case of the $K\beta_{1,3}L^1$ lines in Pb there is a clear separation between the shapes for the $K\beta_3L^1$ and $K\beta_1L^1$ lines, also for the $K\beta_{1,3}L^1$ spectrum for the $1s^{-1}2s^{-1}$ initial states. The sticks generally are distributed similarly in Pb and in Ta, especially in the case of the $K\alpha_1L^1$ and $K\beta_{1,3}L^1$ lines and all the KL^1 spectra for the $1s^{-1}2s^{-1}$ initial states.

Summarizing the results of the detailed analysis of Figs. 2–7, the distance between the $K\alpha_1L^1$ and $K\alpha_2L^1$ bands and between the $K\beta_1L^1$ and $K\beta_3L^1$ bands increases strongly with Z, so that while in Pd, Sn, and Tb the $K\beta_1L^1$ bands are not resolved from the $K\beta_3L^1$ bands, in Ta, Pb, and Th we can observe the appropriate satellite bands separated. It should be added that the distance between the bands of consecutive satellite line kinds (such as, e.g., $K\beta_5L^1$ and $K\beta_2L^1$) also increases with Z. The higher Z, the more widely sticks are distributed in all the satellite spectra and thus the wider shapes of the spectra. Moreover, the shapes of the spectra for the $1s^{-1}2s^{-1}$ initial states are often significantly different from those for the $1s^{-1}2p^{-1}$ initial states. It is also observed that with the increase of Z the shapes of particular spectra tend to be smoother and resemble more the corresponding diagram line shapes. The only exception are the $K\beta_2$ lines. As for any other lines, the $K\beta_2$ diagram lines with the increase of Z become better resolved into two lines ($K\beta_2^{II}$ and $K\beta_2^{I}$), so that they are experimentally separable into the two

TABLE II. Theoretical values of energy shifts (in eV) of average positions of groups of the KL^1 satellite lines with respect to the positions of the appropriate diagram lines. The symbol $1s^{-1}L^{-1}$ concerns the energy shifts corresponding to the KL^1 summary spectra, taking into account statistically added KL^1 transitions from the $1s^{-1}2s^{-1}$ and from the $1s^{-1}2p^{-1}$ states.

Element	Initial states of KL^1 lines	Transition							
		$K\alpha_3$	$K\alpha_2$	$K\alpha_1$	$K\beta_{1,3}$	$K\beta_5$	$K\beta_2$	$K\beta_4$	$KO_{2,3}$
$_{46}$Pd	$1s^{-1}2s^{-1}$	29.8	56.9	53.5	112.4	109.9	138.6	141.9	
	$1s^{-1}2p^{-1}$	84.0	56.1	64.7	141.4	139.6	168.2	171.8	
	$1s^{-1}L^{-1}$	76.2	56.3	61.5	134.3	132.4	160.8	164.6	
$_{50}$Sn	$1s^{-1}2s^{-1}$	33.7	62.9	60.9	126.6	123.1	157.4	160.2	169.6
	$1s^{-1}2p^{-1}$	93.6	61.9	72.8	158.2	155.2	189.5	192.8	202.8
	$1s^{-1}L^{-1}$	84.9	62.2	69.4	150.4	147.4	181.5	184.9	193.9
$_{65}$Tb	$1s^{-1}2s^{-1}$	52.4	90.0	94.8	187.1	181.1	231.2	233.0	247.6
	$1s^{-1}2p^{-1}$	134.9	84.4	108.5	225.9	220.5	271.1	272.8	288.7
	$1s^{-1}L^{-1}$	123.1	86.1	104.6	216.5	210.8	261.3	263.0	278.3
$_{73}$Ta	$1s^{-1}2s^{-1}$	60.8	107.8	118.1	225.2	218.8	275.3	277.1	292.4
	$1s^{-1}2p^{-1}$	156.8	96.9	132.4	266.4	260.1	317.7	319.3	335.1
	$1s^{-1}L^{-1}$	143.0	100.0	128.3	256.5	249.9	307.2	308.8	324.4
$_{82}$Pb	$1s^{-1}2s^{-1}$	73.2	129.8	148.8	273.5	267.0	334.1	336.4	355.8
	$1s^{-1}2p^{-1}$	185.3	109.7	163.1	316.8	314.7	377.0	381.3	398.3
	$1s^{-1}L^{-1}$	169.2	115.5	159.0	306.3	302.3	366.4	369.8	387.7
$_{90}$Th	$1s^{-1}2s^{-1}$	84.0	152.8	183.0	324.3	319.4	395.3	399.2	423.9
	$1s^{-1}2p^{-1}$	212.6	120.8	195.9	366.3	370.9	435.8	439.0	463.8
	$1s^{-1}L^{-1}$	194.1	129.9	192.2	356.2	357.5	425.8	429.1	453.9

bands in the cases of the heaviest studied elements—Ta, Pb, and Th [56]. The $K\beta_2L^1$ lines with the increase of Z are more and more widely distributed. That is why the groups of $K\beta_2^{II}L^1$ and $K\beta_2^{I}L^1$ lines overlap and even in Th the appropriate two bands are not visible. As it can be seen, Th $K\beta_2L^1$ lines retain a rich structure (despite a very large natural linewidth).

B. Energy shifts resulting from the *L*-shell ionization

The groups of satellite lines are shifted in the spectra towards higher energies with respect to the corresponding diagram lines, which originates from the fact that the electron screening of the nuclear charge in multiply ionized atoms is weaker than in singly ionized atoms. A rough estimate of the shifts of the satellite KL^1 lines with respect to the appropriate diagram lines can be performed on the basis of Figs. 2–7. Yet, a more detailed analysis demands the exact values of the energy shifts of the average positions of all the analyzed groups of the KL^1 satellite lines, which are gathered in Table II.

From Table II it can be observed that the higher Z the bigger shifts of all the satellite line groups in the case of the $1s^{-1}2s^{-1}$ and $1s^{-1}2p^{-1}$ initial states and also the summary spectra. As for the energy shifts in the case of each element, it could be predicted that the increase of orbital energies resulting from removing an additional L-shell electron is the bigger, the lower (meaning more negative) energy the respective orbital has. For the orbitals the electrons of which take part in the studied transitions it might be expected that the biggest increase would be for the $1s$ orbital, then $2s$, $2p_{1/2}$, $2p_{3/2}$, $3p_{1/2}$, $3p_{3/2}$, $3d_{3/2}$, $3d_{5/2}$, $4p_{1/2}$, $4p_{3/2}$, $4d_{3/2}$, $4d_{5/2}$, $5p_{1/2}$, and the smallest for $5p_{3/2}$. The energy shift is the higher, the bigger the difference between the amounts of the energy increase for the appropriate two orbitals (depending on the transition). Accordingly, if the above order of the amount of energy increase was correct, the shifts of the groups of the KL^1 satellite lines (with respect to the appropriate diagram lines) would increase with the energy of the corresponding diagram transitions. The shift would be then the biggest for the KO_3L^1 line group (the difference between the increase for the $1s$ and $5p_{3/2}$ orbitals would be the biggest of all) and the smallest for the $K\alpha_3L^1$ line group (the difference between the increase for the $1s$ and $2s$ orbitals would be the smallest of all).

However, it can be seen from Table II that the shifts do not follow exactly the trends expected before obtaining the exact values of the energy shifts. The energy shifts of respective groups of satellite lines accompanying the transitions from the $1s^{-1}2p^{-1}$ states generally increase, according to the energetic order, from the $K\alpha_2L^1$ to $KO_{2,3}L^1$ lines. Yet, there is a break in the increasing trend for Pd, Sn, Tb, Ta, and Pb in the case of the $K\beta_{1,3}L^1$ and $K\beta_5L^1$ lines. For the above elements the $K\beta_5L^1$ lines have a shift being 97–99 % of the shifts of the $K\beta_{1,3}L^1$ lines. Moreover, the case of the $K\alpha_3L^1$ satellite lines for the initial states with a $2p$ hole seems to be especial, as for all the studied elements their shifts are relatively big, stronger than for the $K\alpha_2L^1$ and $K\alpha_1L^1$ lines.

In the case of the transitions from the $1s^{-1}2s^{-1}$ states the trends are a little different. First, the energy shifts of the $K\alpha_3L^1$ satellite lines are the smallest of all the lines. Then, for Tb, Ta, Pb, and Th the shifts increase in the order: $K\alpha_3$, $K\alpha_2$, $K\alpha_1$, $K\beta_5$, $K\beta_{1,3}$, $K\beta_2$, $K\beta_4$, and $KO_{2,3}$ (so with only one break in the energetic order, again between the $K\beta_5$ and $K\beta_{1,3}$ lines). In the case of the lightest studied elements (Pd and Sn) the order of increasing shifts is as follows: $K\alpha_3$, $K\alpha_1$, $K\alpha_2$, $K\beta_5$, $K\beta_{1,3}$, $K\beta_2$, $K\beta_4$, and (only for Sn) $KO_{2,3}$ (so with two breaks in the energetic order, between the $K\alpha_2$ and $K\alpha_1$ lines and between the $K\beta_5$ and $K\beta_{1,3}$ lines).

In the summary spectra the energy shifts follow the same pattern as in the spectra for the $1s^{-1}2p^{-1}$ initial states. Moreover, for all satellite lines apart from $K\alpha_2$, the energy shift of the average position of a line accompanying the transition from the initial state with an additional $2p$ hole is bigger than the shift of the average position of the same line accompanying the transition from the initial state with an additional $2s$ hole. It is also interesting that with increasing Z the shift of the $K\alpha_3L^1$ lines is closer and closer to the $K\alpha_1L^1$ line shift, so that for Pd (in the summary spectra) the $K\alpha_3L^1$ shift is 124% of the $K\alpha_1L^1$ shift, while in Th it is only 101%.

The discrepancies between the described predictions and the actual trends may be partly explained by the fact that the value of mean radius $\langle r\rangle$ of the orbitals important in our studies increases for Pd, Sn, Tb, Ta, and Pb in the order: $1s$, $2p_{1/2}$, $2p_{3/2}$, $2s$, $3d_{3/2}$, $3d_{5/2}$, $3p_{1/2}$, $3p_{3/2}$, $4p_{1/2}$, $4p_{3/2}$, $4d_{3/2}$, $4d_{5/2}$, and (if applicable) $5p_{1/2}$ and $5p_{3/2}$, whereas for Th there is a difference in the case of the M-shell orbitals, for which $\langle r\rangle$ increases in the order: $3d_{3/2}$, $3p_{1/2}$, $3d_{5/2}$ and $3p_{3/2}$. First, such order of all the investigated orbitals justifies the previously mentioned fact that removing a $2p$ electron causes a bigger effect than removing a $2s$ electron. Second, the above order is identical to the order of the declining sensitivity of respective orbitals to removing a $2p$ electron (and thus also of the declining extent of the energy increase). Consequently, the smallest shifts of the groups of the KL^1 lines for the $1s^{-1}2p^{-1}$ initial states (and also the groups in the summary spectra) are observed for the $K\alpha_2L^1$ lines, and then they increase in the order: $K\alpha_1L^1$, $K\alpha_3L^1$, $K\beta_5L^1$, $K\beta_{1,3}L^1$, $K\beta_2L^1$, and $KO_{2,3}L^1$ for Pd, Sn, Tb, Ta, and Pb. In the case of Th the shift of the $K\beta_{1,3}L^1$ lines is smaller than that of the $K\beta_5L^1$ lines.

Removing a $2s$ electron causes similar effects, but it must be considered that the $2s$ orbital is more sensitive to removing a $2s$ electron than the $2p_{1/2}$ and $2p_{3/2}$ orbitals. Thus the shifts of the satellite line kinds for the $1s^{-1}2s^{-1}$ initial states generally increase in the order: $K\alpha_3$, $K\alpha_1$, $K\alpha_2$, $K\beta_5$, $K\beta_{1,3}$, $K\beta_2$, $K\beta_4$, and $KO_{2,3}$. Even Th follows this pattern, in spite of different order of orbital $\langle r\rangle$ values, but it is understandable, as the order in the case of the $3d$ and $3p$ orbitals in Th is not completely reverse to that of other studied elements.

Moreover, there are some exceptions to the above order, concerning the $K\alpha_2L^1$ and $K\alpha_1L^1$ line shifts in the two lightest elements. As it has been noticed before, in Pd and Sn the $K\alpha_1L^1$ shift is smaller than the $K\alpha_2L^1$ shift in the case of the $1s^{-1}2s^{-1}$ initial states. This can be explained on the basis of the j-j coupling model, used in our calculations, which works the better, the higher Z an element has. Thus for the relatively light Pd ($Z=46$) and Sn ($Z=50$) there is in fact a so-called intermediate coupling and significant mixing of the states with the same J occurs. As a result, some satellite lines regarded as of the $K\alpha_2$ kind are in fact a mixture of the $K\alpha_2L^1$ line with the $K\alpha_1L^1$ line (with smaller contribution) and vice versa. This can lead even to the change of the order of the values of the energy shifts for the $K\alpha_2L^1$ and $K\alpha_1L^1$ lines. The mixing coefficients vary significantly with Z, so that for higher Z elements (especially for the heaviest one studied here—Th) it can be assumed that no lines, at least of the $K\alpha_{1,2}L^1$ kind, have any admixture. Thus in the case of the studied elements other than Pd and Sn the energy shift of the $K\alpha_1L^1$ lines for the $1s^{-1}2s^{-1}$ initial states is bigger than that of the $K\alpha_2L^1$ lines. Yet, it should be noted that even for Pd and Sn the j-j coupling model is more adequate than the L-S coupling.

Another observation, previously mentioned, which cannot be explained simply basing on $\langle r\rangle$ values is that the shift of the $K\alpha_2L^1$ line is bigger for the $1s^{-1}2s^{-1}$ initial states than for the $1s^{-1}2p^{-1}$ ones, which is contrary to all the other lines. This may be partly understood by analyzing the $K\alpha_2L^1$ spectrum for the initial states with a $2s$ hole in each of Figs. 2–7, where there is a peak of remarkable intensity on the right side of the $K\alpha_2L^1$ band, i.e., in the energy region where there are no $K\alpha_2L^1$ lines of significant intensities for the initial states with a $2p$ hole. This peak must be the reason for the bigger shift of the average position of the $K\alpha_2L^1$ lines in the case of a $2s$ hole and appears as a result of the fact that in each of the $K\alpha_1L^1$ and $K\alpha_2L^1$ bands for the initial states with a $2s$ hole the sticks are considerably scattered and that the last $K\alpha_2L^1$ stick for the initial states with a $2s$ hole is of high intensity. In the satellite spectrum for the $1s^{-1}2s^{-1}$ initial states the distance between the first and last $K\alpha_1L^1$ line (equal to the distance between the first and last $K\alpha_2L^1$ line) reflects the size of the splitting of the $1s^{-1}2s^{-1}$ initial states, which is quite big [see Figs. 1(b) and 2(a) in Ref. [32]] and is characteristic of each element.

In Table III we have compared the calculated energy shifts with available experimental data and also with the values based on a crude theoretical model by Burch *et al.* [59] and two semiempirical formulas by Török *et al.* [60,61]. It can be observed that our theoretical values are in a good agreement with the experimental ones. The formulas by Burch *et al.* and by Török *et al.* give the values agreeing with ours only in some cases, because each of the formulas works well only for a very restricted range of Z. The values calculated with both formulas by Török *et al.* (for the $K\alpha_{1,2}L^1$ lines [60] and for the $K\beta_{1,3}L^1$ lines [61]) agree with our values only for Pd and Sn. The formulas by Burch *et al.* [59], based on a very crude model, generally describe the investigated energy region poorly and they give the accurate value only in the case of Tb $K\alpha_{1,2}L^1$ lines and a sensible value, though still with clear discrepancy, for Ta $K\alpha_{1,2}L^1$ lines and for Th $K\beta_{1,3}L^1$ lines.

IV. SUMMARY AND CONCLUSIONS

MCDF-MSAL calculations (with the inclusion of the Breit interaction, self-energy, and vacuum polarization cor-

TABLE III. Comparison of some of the values of energy shifts (in eV) of the KL^1 lines: calculated, E_{calc}, with available experimental ones, E_{exp}, and with the values obtained on the basis of two kinds of formulas, E_{Burch} and E_{semi}. E_{Burch} values concern a crude model by Burch *et al.* [59] and E_{semi} values concern one of the two formulas by Török *et al.* (for the $K\alpha_{1,2}L^1$ lines [60] or for the $K\beta_{1,3}L^1$ lines [61]).

Element	Satellite line	E_{calc}	E_{exp}	E_{Burch}	E_{semi}
$_{46}$Pd	$K\alpha_2L^1$	56.3	57[a] ± 5		
			54.4[b] ± 3.9		
	$K\alpha_1L^1$	61.5	62[a] ± 5		
			62.6[b] ± 2.5		
	$K\alpha_{1,2}L^1$	61.8	61[c] ± 2	69.5	59.9
	$K\beta_{1,3}L^1$	134.3	139[d] ± 5	183.3	136.9
			133[c] ± 2		
			136[e] ± 4		
	$K\beta_2L^1$	160.8	165[d] ± 5		
$_{50}$Sn	$K\alpha_{1,2}L^1$	69.1		76.1	66.1
	$K\beta_{1,3}L^1$	150.4		200.8	150.4
$_{65}$Tb	$K\alpha_2L^1$	86.1	81[f] ± 7		
	$K\alpha_1L^1$	104.6	99.2[f] ± 6.0		
			101[g] ± 6		
	$K\alpha_{1,2}L^1$	100.7		101.0	89.0
	$K\beta_{1,3}L^1$	216.5		266.5	201.0
$_{73}$Ta	$K\alpha_1L^1$	128.3	125[h] ± 10		
	$K\alpha_{1,2}L^1$	121.0		114.3	101.2
	$K\beta_{1,3}L^1$	256.5		301.6	227.9
$_{82}$Pb	$K\alpha_{1,2}L^1$	148.5		129.2	115.0
	$K\beta_{1,3}L^1$	306.3		341.0	258.2
$_{90}$Th	$K\alpha_{1,2}L^1$	175.4		142.5	127.2
	$K\beta_{1,3}L^1$	356.2		376.0	285.2

[a]100-MeV ^{16}O ion impact (Ref. [62]).
[b]88.0-MeV ^{16}O ion impact (Ref. [24]).
[c]$^4He^{2+}$ ion impact (Ref. [53]).
[d]26.8-MeV ^{4}He ion impact (Ref. [31]).
[e]88.0-MeV ^{16}O ion impact (Ref. [38]).
[f]210-MeV $^{14}N^{7+}$ ion impact (Ref. [63]).
[g]300-MeV ^{20}Ne ion impact (Ref. [64]).
[h]350-MeV $^{14}N^{7+}$ ion impact (Ref. [63]).

rections) of the positions and intensities of the K x-ray lines have been performed for a wide range of the atomic number (from $Z=46$ to $Z=90$). The results obtained for 11 (for Pd) or 13 (for Sn, Tb, Ta, Pb, and Th) K x-ray diagram lines of the $E1$, $E2$, and $M1$ types are in a good agreement with the experimental ones [55–57]. Our theoretical energies of the KL^1 satellite lines also agree with available experimental data (see Table III).

Removing an L-shell electron, apart from a $1s$ electron, results in a dramatic increase (with respect to the diagram lines) of the number of transitions and also in a wide distribution of the KL^1 satellite lines in the spectra. The theoretical simulation of the spectra as the sum of the Lorentzian natural line shapes with the appropriate natural linewidths enables an investigation of the satellite line shape for each kind of line. It has been found that the shapes of the spectra for the $1s^{-1}2s^{-1}$ initial states are often very different from the shapes of the spectra for the $1s^{-1}2p^{-1}$ initial states. Generally, for a given element the shapes of the KL^1 spectra for the initial states with a $2s$ hole are more different from the shapes of the corresponding diagram lines than the shapes of the KL^1 spectra for the initial states with a $2p$ hole. Moreover, there are gradual changes of the shapes and structure of the KL^1 spectra with the increase of Z, though generally there are many differences in the shapes and structures between the elements. The distribution of particular sticks in the KL^1 spectra is the wider, the higher Z of the element. It has been observed that with increasing Z the shapes of the KL^1 lines (apart from the $K\beta_2L^1$ lines) become smoother and they also tend to resemble more and more the shapes of the appropriate diagram lines.

The analysis of the energy shifts of average positions of the KL^1 satellite lines with respect to the corresponding diagram lines has shown that the shifts follow similar trends for all the studied elements. The particular line groups have bigger shifts when the hole is in the $2p$ subshell than when it is

in the $2s$ subshell in all the cases apart from the $K\alpha_2L^1$ lines. This fact can be justified by $\langle r\rangle$ value, which is smaller for the $2p$ orbital than for the $2s$ orbital and thus removing a $2p$ electron has a more significant effect on the increase of the orbital energy than removing a $2s$ electron. The obtained order of increasing shifts for a given element (which was supposed to be in agreement with the order of increasing line energies) has appeared to be a little surprising, but it can be qualitatively explained mainly on the basis of $\langle r\rangle$ values. What seems especially interesting is that the shifts of the $K\beta_5L^1$ lines are smaller than those of the $K\beta_{1,3}L^1$ lines (for all the elements studied apart from the heaviest Th) and that the shift of the $K\alpha_3L^1$ lines for the states with a $2p$ hole (and thus also of the $K\alpha_3L^1$ lines in the summary spectra) is for each investigated element bigger than those of the $K\alpha_1L^1$ and $K\alpha_2L^1$ lines.

Both the results of the calculations and their analysis presented in this paper make a systematic study which examines in detail and explains various aspects of the structure and shapes of the spectra of many different satellite KL^1 x-ray lines and concerns a wide range of the atomic number. It is also worth emphasizing that our investigation considers apart from strong $E1$ diagram and satellite lines also weak lines of this type and the lines of other types ($E2$ and $M1$). The authors believe that the results of their analysis will be very helpful in reliable and quantitative interpretation of the K x-ray spectra of Pd, Sn, Tb, Ta, Pb, and Th induced by various projectiles, which will be measured in the future or which have already been measured but could not be successfully analyzed. It is also worth mentioning that our research will contribute to better understanding of collision processes, by enabling obtaining reliable data about the ionization of the L shell of target atoms (in collisions with light or heavy projectiles). These data will be very valuable in testing and improving various theoretical models describing the course of collision processes (e.g., plane-wave Born approximation, semiclassical approximation, classical trajectory Monte Carlo). Moreover, our results can be of vital importance in designing new experiments, involving elements studied here and other elements having the x-ray spectra in a similar energy range.

ACKNOWLEDGMENTS

This work has been financially supported by the Polish Committee for Scientific Research (KBN) under Grant No. 2 P03B 094 24 awarded for the period of 2003–2006 and Grant No. 1 P03B 021 26 awarded for the period of 2004–2006.

APPENDIX

Here we analyze in detail the results of the calculations of the positions and intensities of the studied K x-ray diagram lines of Pd, Tb, Pb, and Th, presented in Table I. From the comparison of the calculated values of energies it can be observed that, as should be expected, with the increase of Z transition energies increase significantly (depending on the line, by about 70–85 keV with the increase of Z from $Z=46$ to $Z=90$). It is understandable because if an electron is removed from a neutral atom, the energies of the levels increase with respect to the appropriate energies in the neutral atom. The highest relative energy increase is in the case of the K x-ray level (i.e., the $1s^{-1}$ states), as the amount of energy needed to remove an electron from this level is the biggest. Then the relative energy increase of the levels important in our studies declines in the order: $2s^{-1}$, $2p_{1/2}^{-1}$, $2p_{3/2}^{-1}$, $3p_{1/2}^{-1}$, $3p_{3/2}^{-1}$, $3d_{3/2}^{-1}$, $3d_{5/2}^{-1}$, $4p_{1/2}^{-1}$, $4p_{3/2}^{-1}$, $4d_{3/2}^{-1}$, $4d_{5/2}^{-1}$, $5p_{1/2}^{-1}$, and $5p_{3/2}^{-1}$ (see Fig. 1). The relative energy increase of each x-ray level is the bigger, the higher Z. Thus the biggest increase of transitions energies with Z will be observed in the case of the transition between the levels for which the amounts of relative energy increase due to the ionization differ most. Consequently, the energy of the KO_3 transition increases most with Z (because the relative energy increase of the final, $5p_{3/2}^{-1}$, level is the smallest of all the levels studied), while the energy of the $K\alpha_3$ transition increases least (as the relative energy increase of the final, $2s^{-1}$, level is the second biggest after the $1s^{-1}$ level).

It can also be seen from Table I, again as we should anticipate, that the lines of the $E1$ type (i.e., $K\alpha_2$, $K\alpha_1$, $K\beta_3$, $K\beta_1$, $K\beta_2^{II}$, $K\beta_2^{I}$, KO_2, and KO_3) are much stronger than the lines of the $E2$ type ($K\beta_5^{II}$, $K\beta_5^{I}$, $K\beta_4^{II}$, and $K\beta_4^{I}$) and of the $M1$ type ($K\alpha_3$). For example, the $K\alpha_1$ line ($E1$) is 200–1300 times (depending on Z) stronger than the $K\beta_5^{I}$ line ($E2$) and 500–52 500 times stronger than the $K\alpha_3$ line ($M1$). The $K\beta_5^{I}$ line is thus 2.5–40 times stronger than the $K\alpha_3$ line. Within the $E1$ type the most intense are the $K\alpha_{1,2}$ lines and then in turn: $K\beta_{1,3}$, $K\beta_2$, and $KO_{2,3}$. In each of these pairs of lines the lines of higher energies, for which $\Delta l=-1$ and $\Delta J=1$, are stronger. These lines are: $K\alpha_1$, $K\beta_1$, $K\beta_2^{I}$, and KO_3. For the weaker lines from each pair (i.e., $K\alpha_2$, $K\beta_3$, $K\beta_2^{II}$, and KO_2) $\Delta l=-1$ and $\Delta J=0$. Within the $E2$ type the $K\beta_5$ lines are more intense than the $K\beta_4$ lines and in both these pairs the lines of higher energies ($K\beta_5^{I}$ and $K\beta_4^{I}$), where $\Delta l=-2$ and $\Delta J=2$, are stronger. For the weaker lines ($K\beta_5^{II}$ and $K\beta_4^{II}$) $\Delta l=-2$ and $\Delta J=1$. Thus among the investigated lines of the same type ($E1$ or $E2$) the intensity is the stronger from the more inner shell the transition takes place. Moreover, the most probable among the transitions from the same shell are those where J changes by the same amount as l, but in the opposite direction than l. This may be explained by the statistical reasons, since the stronger transitions in each pair are from the states with higher J quantum number than the weaker transitions.

From the performed calculations it can be observed that, as should be expected, with increasing Z absolute intensities I_a of all the diagram lines increase, e.g., for the $K\alpha_1$ line of Pd $I_a=4.1206\times10^{15}$, while for Th $I_a=5.2788\times10^{16}$ (the values of I_a have been calculated using Coulomb gauge [45] and give the number of transitions per second). From Table I it can be noticed that also relative (with respect to the $K\alpha_1$ line) intensities of all the lines increase with Z. The most conspicuous relative increase with Z of the intensity with respect to the $K\alpha_1$ line is for the $K\alpha_3$ ($M1$) line, which is the weakest of all the investigated lines in Pd, Sn, Tb, and Ta, whereas in Pb it is stronger than the $K\beta_4^{II}$ line and in Th—stronger than

each of the $K\beta_4$ lines. The intensities of the $E2$ lines with respect to the appropriate $K\alpha_1$ lines also significantly increase with Z, more (relatively) in the case of the $K\beta_4$ lines than for the $K\beta_5$ lines. Remarkably smaller relative increase with Z of the intensity with respect to the $K\alpha_1$ line can be observed for the majority of the $E1$ lines (with the exception of the $KO_{2,3}$ lines, where the increase is quite large). Thus the heavier the atom, the more important the transitions of the $M1$ and $E2$ types and transitions of different types from high shells (which is connected with relativistic effects, whose role increases with Z). In addition, as could be anticipated, the increasing role of relativistic effects causes the distance between the diagram lines in the same pair (i.e., accompanying the transitions from the same nonrelativistic subshell, like, e.g., the $K\alpha_1$ and $K\alpha_2$ lines) to strongly increase with Z. For each element the distance between the lines from such pairs of lines is the bigger from the more inner shell the transition takes place, thus it is the greatest for the $K\alpha_1$ and $K\alpha_2$ lines, which are at the same time the easiest to resolve in the spectra.

[1] P. Richard, I. L. Morgan, T. Furuta, and D. Burch, Phys. Rev. Lett. **23**, 1009 (1969).
[2] A. R. Knudson, D. J. Nagel, P. G. Burkhalter, and K. L. Dunning, Phys. Rev. Lett. **26**, 1149 (1971).
[3] D. Burch, P. Richard, and R. L. Blake, Phys. Rev. Lett. **26**, 1355 (1971).
[4] D. G. McCrary and P. Richard, Phys. Rev. A **5**, 1249 (1972).
[5] D. G. McCrary, M. Senglaub, and P. Richard, Phys. Rev. A **6**, 263 (1972).
[6] C. F. Moore, M. Senglaub, B. Johnson, and P. Richard, Phys. Lett. **40A**, 107 (1972).
[7] P. G. Burkhalter, A. R. Knudson, D. J. Nagel, and K. L. Dunning, Phys. Rev. A **6**, 2093 (1972).
[8] C. F. Moore, D. K. Olsen, B. Hodge, and P. Richard, Z. Phys. **257**, 288 (1972).
[9] R. L. Kauffman, J. H. McGuire, P. Richard, and C. F. Moore, Phys. Rev. A **8**, 1233 (1973).
[10] T. K. Li, R. L. Watson, and J. S. Hansen, Phys. Rev. A **8**, 1258 (1973).
[11] P. Richard, R. L. Kauffman, J. H. McGuire, C. F. Moore, and D. K. Olson, Phys. Rev. A **8**, 1369 (1973).
[12] J. McWherter, J. Bolger, C. F. Moore, and P. Richard, Z. Phys. **263**, 283 (1973).
[13] F. Hopkins, D. O. Elliot, C. P. Bhalla, and P. Richard, Phys. Rev. A **8**, 2952 (1973).
[14] R. L. Watson, F. E. Jenson, and T. Chiao, Phys. Rev. A **10**, 1230 (1974).
[15] A. R. Knudson, P. G. Burkhalter, and D. J. Nagel, Phys. Rev. A **10**, 2118 (1974).
[16] R. L. Kauffman, C. W. Wood, K. A. Jamison, and P. Richard, Phys. Rev. A **11**, 872 (1975).
[17] K. W. Hill, B. L. Doyle, S. M. Shafroth, D. H. Madison, and R. D. Deslattes, Phys. Rev. A **13**, 1334 (1976).
[18] J. A. Demarest and R. L. Watson, Phys. Rev. A **17**, 1302 (1978).
[19] C. Schmiedekamp, B. L. Doyle, T. J. Gray, R. K. Gardner, K. A. Jamison, and P. Richard, Phys. Rev. A **18**, 1892 (1978).
[20] R. L. Watson, B. I. Sonobe, J. A. Demarest, and A. Langenberg, Phys. Rev. A **19**, 1529 (1979).
[21] T. Tonuma, Y. Awaya, T. Kambara, H. Kumagai, I. Kohno, and S. Özkök, Phys. Rev. A **20**, 989 (1979).
[22] R. L. Watson, J. R. White, A. Langenberg, R. A. Kenefick, and C. C. Bahr, Phys. Rev. A **22**, 582 (1980).
[23] B. Perny, J.-Cl. Dousse, M. Gasser, J. Kern, Ch. Rhême, P. Rymuza, and Z. Sujkowski, Phys. Rev. A **36**, 2120 (1987).
[24] P. Rymuza, Z. Sujkowski, M. Carlen, J.-Cl. Dousse, M. Gasser, J. Kern, B. Perny, and Ch. Rhême, Z. Phys. D: At., Mol. Clusters **14**, 37 (1989).
[25] R. Salziger, G. L. Borchert, D. Gotta, O. W. B. Schult, D. H. Jakubassa-Amundsen, P. A. Amundsen, and K. Rashid, J. Phys. B **22**, 821 (1989).
[26] D. F. Anagnostopoulos, G. L. Borchert, D. Gotta, and K. Raschid, Z. Phys. D: At., Mol. Clusters **18**, 139 (1991).
[27] D. F. Anagnostopoulos, G. L. Borchert, and D. Gotta, J. Phys. B **25**, 2771 (1992).
[28] P. Rymuza, T. Ludziejewski, Z. Sujkowski, M. Carlen, J.-Cl. Dousse, M. Gasser, J. Kern, and Ch. Rhême, Z. Phys. D: At., Mol. Clusters **23**, 81 (1992).
[29] T. Ludziejewski, P. Rymuza, Z. Sujkowski, D. Anagnostopoulos, G. Borchert, M. Carlen, J.-Cl. Dousse, J. Hoszowska, J. Kern, and Ch. Rhême, Acta Phys. Pol. B **25**, 699 (1994).
[30] M. Carlen, J.-Cl. Dousse, M. Gasser, J. Kern, Ch. Rhême, P. Rymuza, Z. Sujkowski, and D. Trautmann, Europhys. Lett. **13**, 231 (1990).
[31] M. Carlen, J.-Cl. Dousse, M. Gasser, J. Hoszowska, J. Kern, Ch. Rhême, P. Rymuza, Z. Sujkowski, and D. Trautmann, Z. Phys. D: At., Mol. Clusters **23**, 71 (1992).
[32] M. Polasik, Phys. Rev. A **39**, 616 (1989).
[33] M. Polasik, Phys. Rev. A **39**, 5092 (1989).
[34] M. Polasik, Phys. Rev. A **40**, 4361 (1989).
[35] M. Polasik, Phys. Rev. A **41**, 3689 (1990).
[36] M. Polasik, Phys. Rev. A **52**, 227 (1995).
[37] M. W. Carlen, M. Polasik, B. Boschung, J.-Cl. Dousse, M. Gasser, Z. Halabuka, J. Hoszowska, J. Kern, B. Perny, Ch. Rhême, P. Rymuza, and Z. Sujkowski, Phys. Rev. A **46**, 3893 (1992).
[38] M. W. Carlen, B. Boschung, J.-Cl. Dousse, Z. Halabuka, J. Hoszowska, J. Kern, Ch. Rhême, M. Polasik, P. Rymuza, and Z. Sujkowski, Phys. Rev. A **49**, 2524 (1994).
[39] T. Ludziejewski, P. Rymuza, Z. Sujkowski, B. Boschung, J.-Cl. Dousse, B. Galley, Z. Halabuka, Ch. Herren, J. Hoszowska, J. Kern, Ch. Rhême, and M. Polasik, Phys. Rev. A **52**, 2791 (1995).
[40] T. Ludziejewski, P. Rymuza, Z. Sujkowski, G. Borchert, J.-Cl. Dousse, Ch. Rhême, and M. Polasik, Phys. Rev. A **54**, 232 (1996).
[41] Ch. Herren, B. Boschung, J.-Cl. Dousse, B. Galley, J. Hoszowska, J. Kern, Ch. Rhême, M. Polasik, T. Ludziejewski, P. Rymuza, and Z. Sujkowski, Phys. Rev. A **57**, 235 (1998).
[42] J. Rzadkiewicz, D. Chmielewska, A. Gójska, Z. Sujkowski, M.

Berset, J-Cl. Dousse, Y.-P. Maillard, O. Mauron, P.-A. Raboud, M. Polasik, J. Hoszowska, and M. Pajek, Nucl. Instrum. Methods Phys. Res. B **205**, 128 (2003).
[43] J. Rzadkiewicz, D. Chmielewska, Z. Sujkowski, J.-Cl. Dousse, D. Castella, D. Corminboeuf, J. Hoszowska, P. A. Raboud, M. Polasik, K. Słabkowska, and M. Pajek, Phys. Rev. A **68**, 032713 (2003).
[44] V. L. Kravchuk, A. M. van den Berg, F. Fleurot, M. A. de Huu, H. Löhner, H. W. Wilschut, M. Polasik, M. Lewandowska-Robak, and K. Słabkowska, Phys. Rev. A **64**, 062710 (2001).
[45] I. P. Grant, J. Phys. B **7**, 1458 (1974).
[46] I. P. Grant, B. J. McKenzie, P. H. Norrington, D. F. Mayers, and N. C. Pyper, Comput. Phys. Commun. **21**, 207 (1980).
[47] B. J. McKenzie, I. P. Grant, and P. H. Norrington, Comput. Phys. Commun. **21**, 233 (1980).
[48] I. P. Grant and B. J. McKenzie, J. Phys. B **13**, 2671 (1980).
[49] J. Hata and I. P. Grant, J. Phys. B **16**, 3713 (1983).
[50] I. P. Grant, Int. J. Quantum Chem. **25**, 23 (1984).
[51] K. G. Dyall, I. P. Grant, C. T. Johnson, F. A. Parpia, and E. P. Plummer, Comput. Phys. Commun. **55**, 425 (1989).
[52] F. Parpia, C. Froese Fischer, and I. P. Grant, Comput. Phys. Commun. **94**, 249 (1996).
[53] B. Boschung, M. W. Carlen, J.-Cl. Dousse, B. Galley, Ch. Herren, J. Hoszowska, J. Kern, Ch. Rhême, T. Ludziejewski, P. Rymuza, Z. Sujkowski, and Z. Halabuka, Phys. Rev. A **52**, 3889 (1995).
[54] F. A. Babushkin, Acta Phys. Pol. **25**, 749 (1964).
[55] R. B. Firestone, V. S. Shirley, C. M. Baglin, S. Y. F. Chu, and J. Zipkin, *Table of Isotopes*, 8th Edition (John Wiley & Sons, New York, 1996), Appendix F.
[56] J. A. Bearden, Rev. Mod. Phys. **39**, 78 (1967).
[57] R. D. Deslattes, E. G. Kessler, Jr., P. Indelicato, L. de Billy, E. Lindroth, and J. Anton, Rev. Mod. Phys. **75**, 35 (2003), and references therein.
[58] J. L. Campbell and T. Papp, At. Data Nucl. Data Tables **77**, 1 (2001).
[59] D. Burch, L. Wilets, and W. E. Meyerhof, Phys. Rev. A **9**, 1007 (1974).
[60] I. Török, T. Papp, and S. Raman, Nucl. Instrum. Methods Phys. Res. B **150**, 8 (1999).
[61] I. Török, T. Papp, and S. Raman, Atomki Annual Report, Debrecen, Hungary, 1999, p. 38.
[62] B. Perny, J.-Cl. Dousse, M. Gasser, J. Kern, R. Lanners, Ch. Rhême, and W. Schwitz, Nucl. Instrum. Methods Phys. Res. A **267**, 120 (1988).
[63] D. F. Anagnostopoulos, G. Borchert, D. Gotta, K. Rashid, D. H. Jakubassa-Amundsen, and P. A. Amundsen, Phys. Rev. A **58**, 2797 (1998).
[64] T. Ludziejewski, J. Hoszowska, P. Rymuza, Z. Sujkowski, D. Anagnostopoulos, G. Borchert, M. Carlen, J.-Cl. Dousse, Ch. Rhême, and A. G. Drentje, Nucl. Instrum. Methods Phys. Res. B **63**, 494 (1992).